remote sensing

MDPI

Supplementary Materials

Understanding How Low-Level Clouds and Fog Modify the Diurnal Cycle of Orographic Precipitation Using In Situ and Satellite Observations. *Remote Sensing* 2017, *9*, 920

Yajuan Duan and Ana P. Barros *

Department of Civil and Environmental Engineering, Duke University, Durham, NC 27708, USA; yajuan.duan@duke.edu

* Correspondence: barros@duke.edu; Tel.: +1-919-660-5539

Received: 26 July 2017; Accepted: 30 August 2017; Published: 2 September 2017

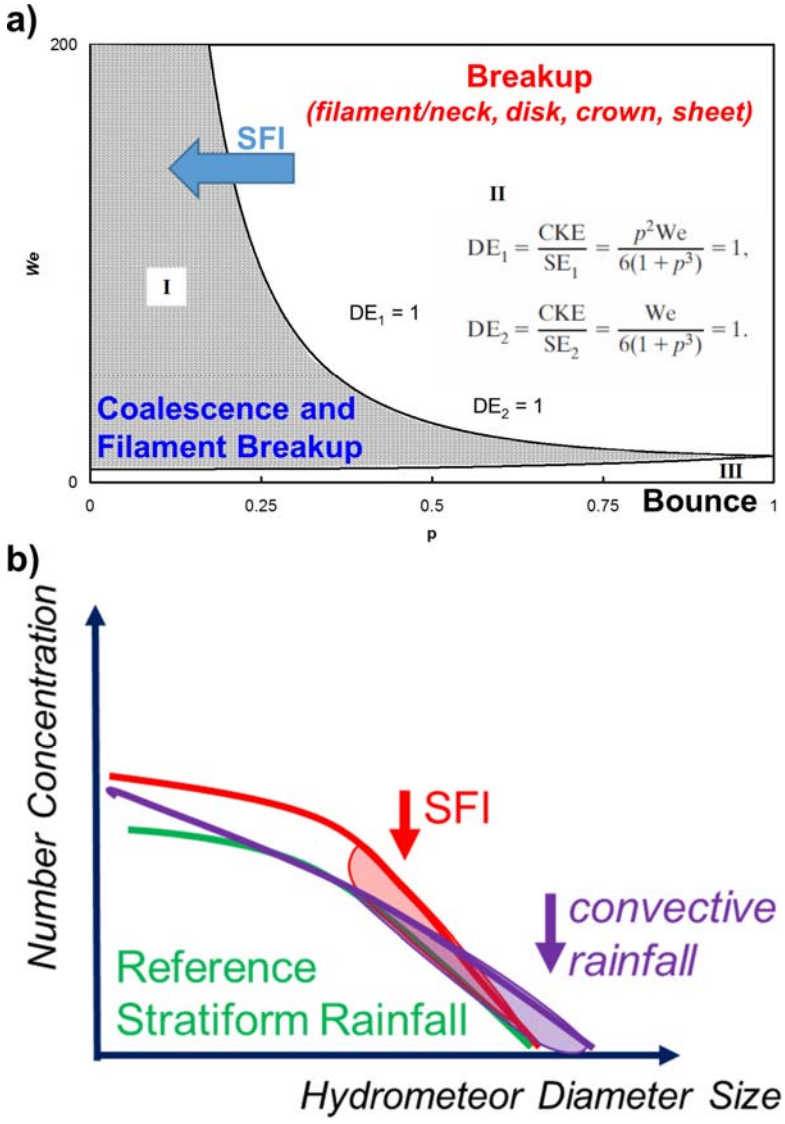

Figure S1. (**a**) Regimes of drop collisions delineated according to DE_1 and DE_2: I-Coalescence and Filament Breakup dominate; II-Breakup dominates; III-Drops collide and bounce. Note SE is the surface tension energy neglecting viscosity, CKE is the collision kinetic energy, p is the diameter ratio between the small and larger diameters of two colliding hydrometeors, and *We* is the Weber number.

This figure is adapted from Testik et al. [1]. For details see Testik [2], Testik et al. [1], Prat et al. [3]; (**b**) Conceptual synthesis of seeder-feeder interactions (SFI) impacts on rain drop size distribution (R-DSD) vis-à-vis convective rainfall of the same intensity with respect to a reference light stratiform rainfall.

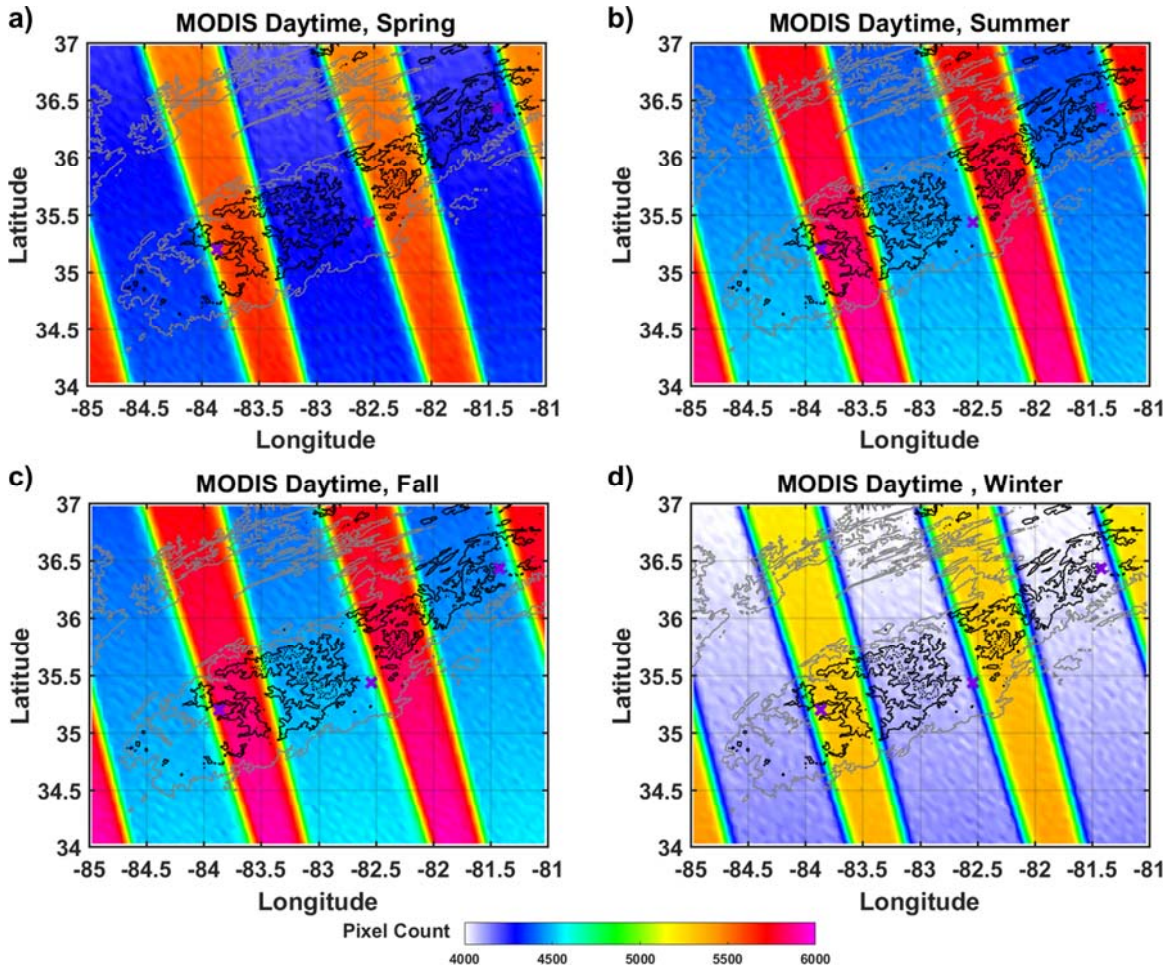

Figure S2. Spatial distributions of MODIS pixel counts with viewing angle less than 20° in each season (spring: April-May-June, summer: July-August-September, fall: October-November-December, and winter: January-February-March) during daytime overpasses of June 2006–October 2016. Note the three ground ceilometer sites (from left to right: KRHP, KAVL, and KGEV) are marked by purple crosses.

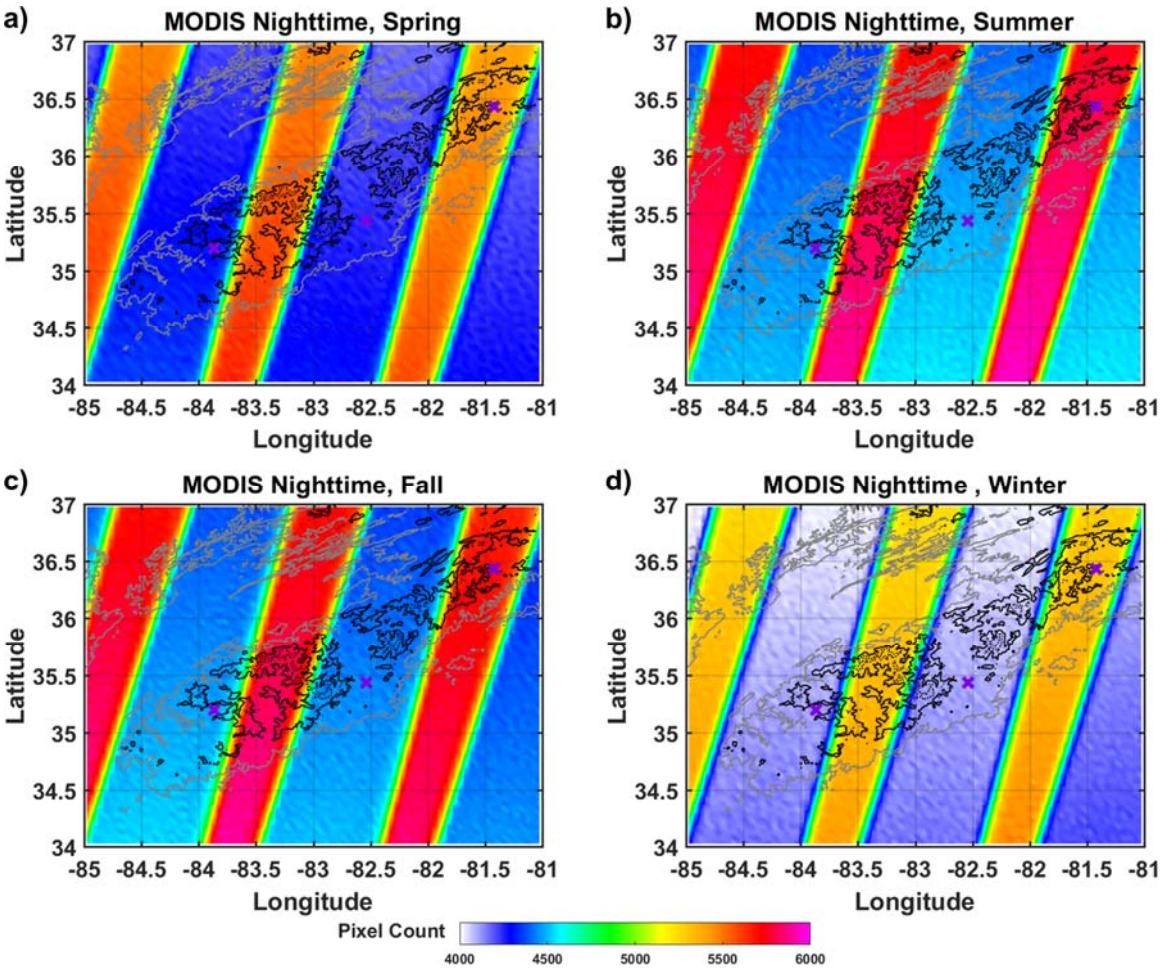

Figure S3. Spatial distributions of MODIS pixel counts with viewing angle less than 20° in each season (spring: April-May-June, summer: July-August-September, fall: October-November-December, and winter: January-February-March) during nighttime overpasses of June 2006–October 2016. Note the three ground ceilometer sites (from left to right: KRHP, KAVL, and KGEV) are marked by purple crosses.

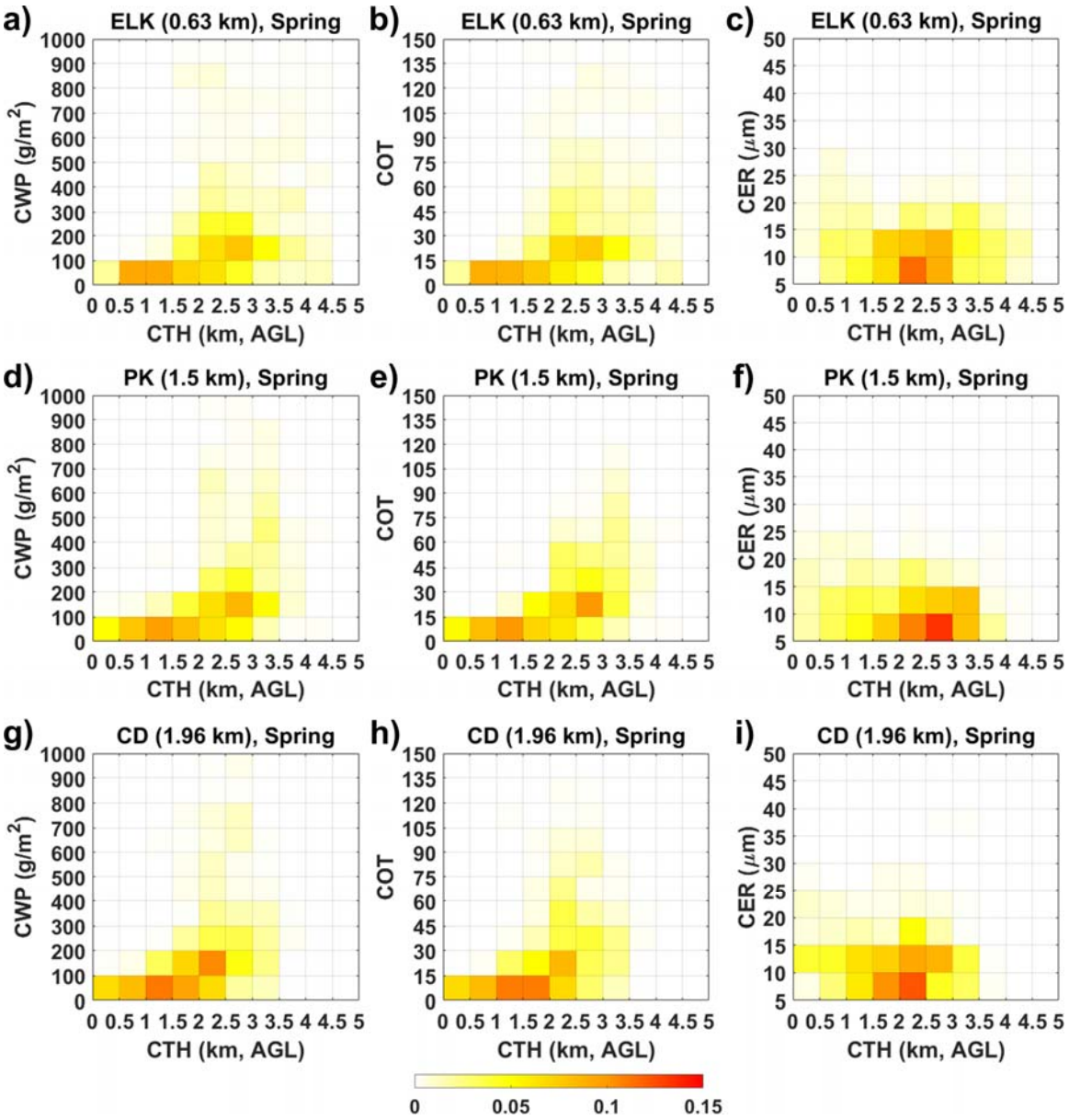

Figure S4. Fractional occurrences of MODIS optical and microphysical properties (CWP, COT, and CER) for single-layered LLCF (CTH < 5 km MSL and viewing angle < 20°) as a function of MODIS CTH (AGL) observed in the grid box (0.05° × 0.05°) where each fog collector is located (ELK: **a–c**, PK: **d–f**, and CD: **g–i**) during the spring of June 2006–October 2016 (daytime overpasses only). Note the elevation of each site is denoted in parentheses after its name.

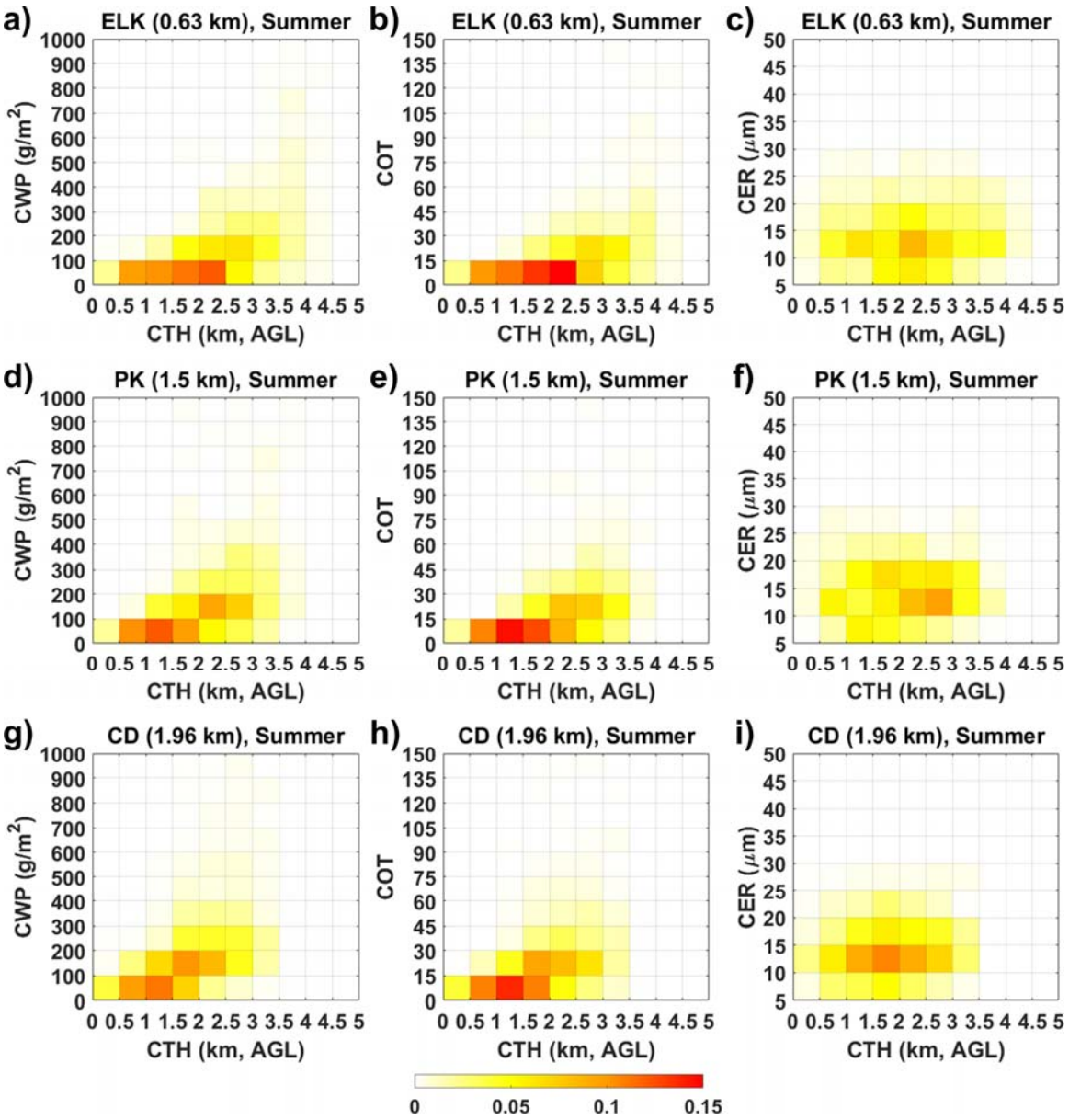

Figure S5. Fractional occurrences of MODIS optical and microphysical properties (CWP, COT, and CER) for single-layered LLCF (CTH < 5 km MSL and viewing angle < 20°) as a function of MODIS CTH (AGL) observed in the grid box (0.05° × 0.05°) where each fog collector is located (ELK: **a–c**, PK: **d–f**, and CD: **g–i**) during the summer of June 2006–October 2016 (daytime overpasses only). Note the elevation of each site is denoted in parentheses after its name.

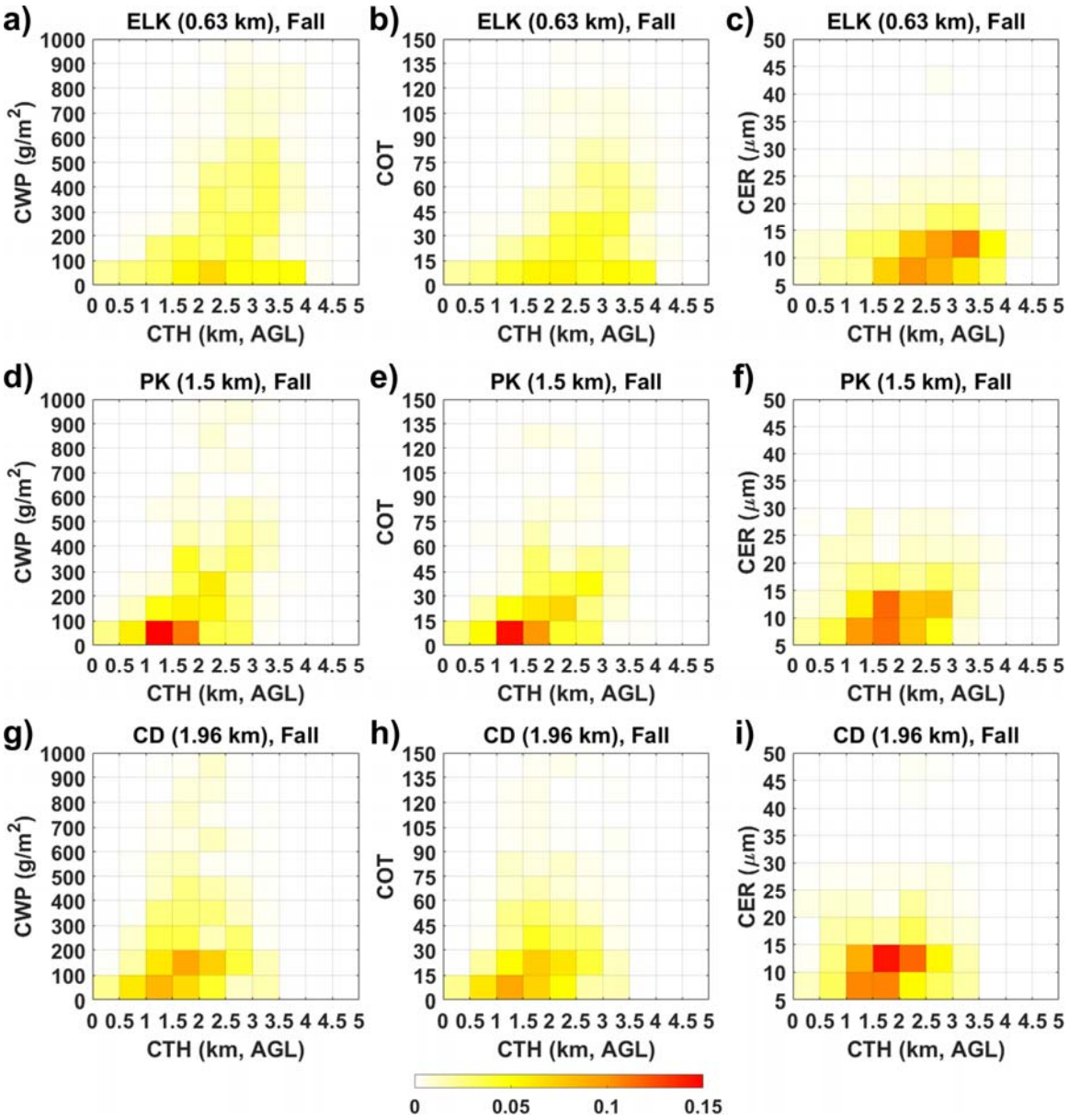

Figure S6. Fractional occurrences of MODIS optical and microphysical properties (CWP, COT, and CER) for single-layered LLCF (CTH < 5 km MSL and viewing angle < 20°) as a function of MODIS CTH (AGL) observed in the grid box (0.05° × 0.05°) where each fog collector is located (ELK: **a–c**, PK: **d–f**, and CD: **g–i**) during the fall of June 2006–October 2016 (daytime overpasses only). Note the elevation of each site is denoted in parentheses after its name.

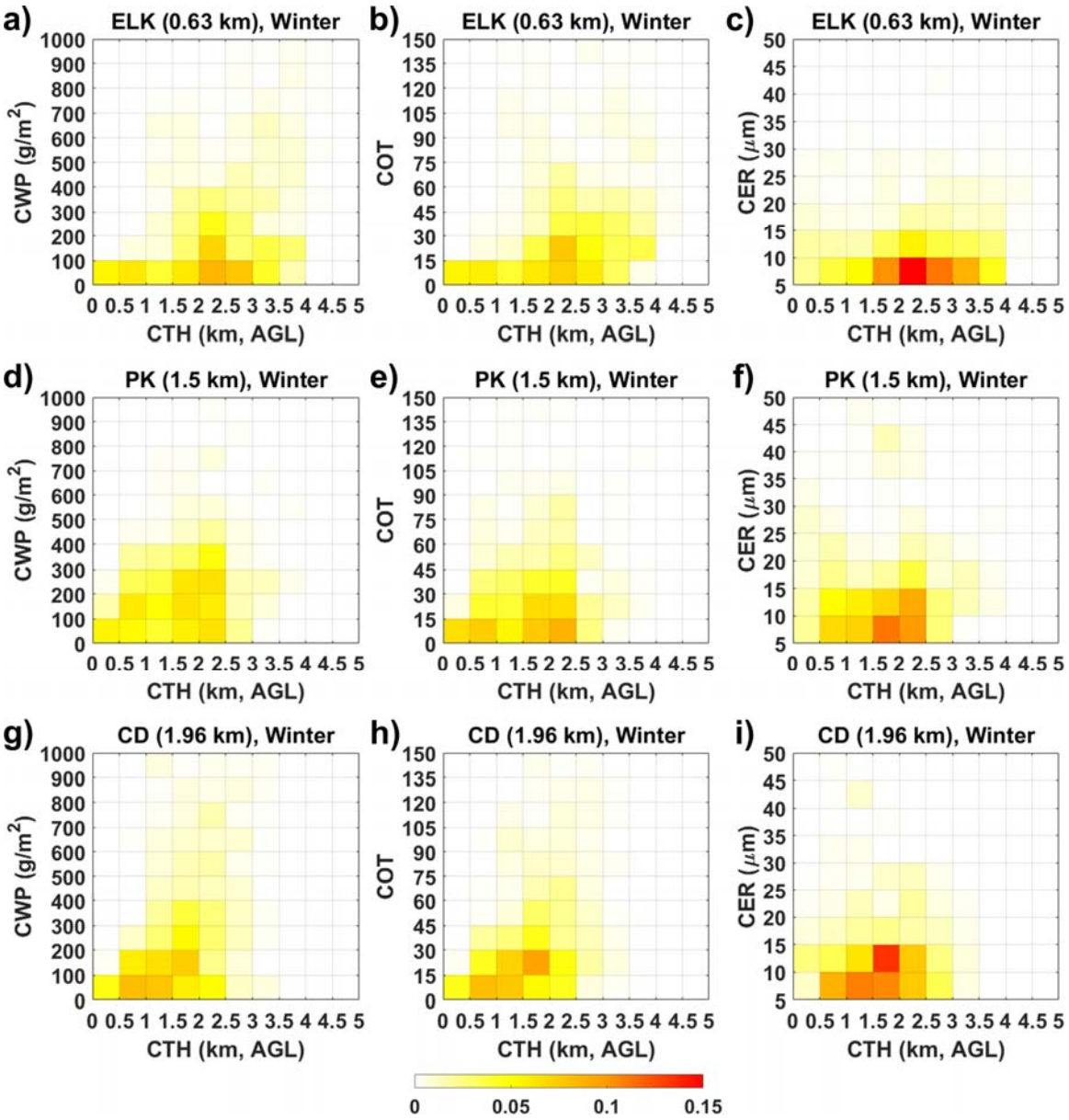

Figure S7. Fractional occurrences of MODIS optical and microphysical properties (CWP, COT, and CER) for single-layered LLCF (CTH < 5 km MSL and viewing angle < 20°) as a function of MODIS CTH (AGL) observed in the grid box (0.05° × 0.05°) where each fog collector is located (ELK: **a–c**, PK: **d–f**, and CD: **g–i**) during the winter of June 2006–October 2016 (daytime overpasses only). Note the elevation of each site is denoted in parentheses after its name.

References

1. Testik, F.Y.; Barros, A.P.; Bliven, L.F. Toward a physical characterization of raindrop collision outcome regimes. *J. Atmosph. Sci.* **2011**, *68*, 1097–1113.
2. Testik, F.Y. Outcome regimes of binary raindrop collisions. *Atmosph. Res.* **2009**, *94*, 389–399.
3. Prat, O.P.; Barros, A.P.; Testik, F.Y. On the influence of raindrop collision outcomes on equilibrium drop size distributions. *J. Atmosph. Sci.* **2012**, *69*, 1534–1546.